



MATERIALS CHEMISTRY

FRONTIERS



CHINESE
CHEMICAL
SOCIETY



ROYAL SOCIETY
OF CHEMISTRY

rsc.li/frontiers-materials

RESEARCH ARTICLE

View Article Online
View Journal | View IssueCite this: *Mater. Chem. Front.*,
2023, 7, 216

Engineered mesoporous silica-based nanoparticles as smart chemotherapy nanodevice for bortezomib administration†

M. De Santo,^a A. Giovinazzo,^b M. Fava,^a E. Mazzotta,^c I. E. De Napoli,^b M. Greco,^a A. Comandé,^a A. Nigro,^a P. Argurio,^{id} I. Perrotta,^d M. Davoli,^d A. Tagarelli,^e R. Elliani,^e T. Granato,^b G. Nicolini,^c A. Chiorazzi,^c S. Semperboni,^c E. Ballarini,^c C. Crocamo,^c G. Cavaletti,^c D. Lombardo,^f D. Sisci,^a C. Morelli ‡,^a A. Leggio ^{id} ‡*^a and L. Pasqua ^{id} ‡*^b

Adverse reactions, toxicity, and poor compliance from patients still represent major challenges for conventional chemotherapy treatments. Localized drug delivery would ideally improve therapeutic efficacy, minimizing the side effects. An MSU-type mesoporous silica-based nanodevice (FOL-MSN-BTZ), able to selectively deliver the antineoplastic drug bortezomib (BTZ) to folate receptor over-expressing multiple myeloma (FR+ MM) cells is described. The receptor-specific ligand, folic acid, grafted on the external surface of the nanosystem, allows tumor recognition and cell internalization, while BTZ, mainly linked to the pore internal surface through a covalent pH-sensitive bond, is released in an acidic tumor environment. A detailed investigation showed that only the fine balancing of different functionalities of the nanodevice around the external and internal surfaces of MSN particles shows the absence of toxicity towards healthy cells *in vitro* and negligible BTZ-release at physiological pH, which are suitable features for applicative purposes in the engineering of therapies. After complete characterization *in vitro*, an accurate suspendability assessment, which considered the sedimentation process that reduces the particle amount and, consequently, drug content in the suspensions, allowed the development of an injectable formulation of FOL-MSN-BTZ that showed higher antitumor efficacy and an overall tendency to lower toxicity in a MM mice model compared to the conventional bortezomib chemotherapy.

Received 4th October 2022,
Accepted 5th November 2022

DOI: 10.1039/d2qm01009g

rsc.li/frontiers-materials

Introduction

The main challenge of modern anticancer medicine is to exclusively address drugs to cancer tissue without affecting normal tissues, thus reducing side effects and maximizing therapeutic efficacy. This ambitious project embraces materials science, chemistry, biology, pharmacology, and medicine, resulting in the engineering of smart nanosystems, which offer unparalleled opportunities to treat various diseases such as cancer.

The wide potentialities in the functionalization of material surfaces allow the versatile developments of tailor-made nanostructured platforms for several biomedical applications, modulating biological response, and improving biocompatibility, therapeutic performance, and selectivity toward specific targets.^{1,2} Inorganic materials appear as promising platforms to meet technical needs for the development of nanodevices for nanomedicine applications. In this context, mesoporous silica nanoparticles (MSNs) have been broadly tested as starting architectures for biomedical applications.^{3,4}

^a Department of Pharmacy, Health and Nutritional Sciences, University of Calabria, via P. Bucci, 87036 Arcavacata di Rende, CS, Italy.

E-mail: antonella.leggio@unical.it

^b Department of Environmental Engineering University of Calabria, via P. Bucci, cubo 44/A, 87036, Arcavacata di Rende, CS, Italy. E-mail: l.pasqua@unical.it; Fax: +39 0984 496655; Tel: +39 0984 496642^c Experimental Neurology Unit, School of Medicine and Surgery and Milan Center for Neuroscience, University of Milano-Bicocca, via Cadore 48, 20900 Monza, Italy^d Department of Biology, Ecology and Earth Sciences, Centre for Microscopy and Microanalysis (CM2), Transmission Electron Microscopy Laboratory, University of Calabria, via P. Bucci, 87036 Arcavacata di Rende, CS, Italy^e Department of Chemistry and Chemical Technologies, University of Calabria, via P. Bucci, 87036 Arcavacata di Rende, CS, Italy^f Institute for Chemical-Physical Processes, National Research Council, 98158 Messina, Italy† Electronic supplementary information (ESI) available. See DOI: <https://doi.org/10.1039/d2qm01009g>

‡ Equally share the last authorship.



Their solid framework, nanostructured through different organic functionalities, provides hybrid organic–inorganic nanodevices able to interact with biological structures,⁵ triggering cell internalization⁶ and drug release, as a response to several stimuli.⁷

MSNs have several advantages, such as high stability, good biocompatibility, regularly sized pores and tunable pore diameter in the range of 15–100 Å, large loading capacity, and ease of surface functionalization.^{8,9} The availability of two different functionalizable surfaces, one internal and the other external to the pores, makes them desirable options for encapsulating therapeutic/diagnostic (theranostic) agents (*e.g.*, drugs, miRNA, siRNA, proteins, enzymes, DNA, as well as probes for imaging applications) to be delivered to the desired target (*e.g.* tumors)^{10,11} These features endorse MSN exploitation in the field of personalized medicine.¹²

Moreover, silica is classified by FDA as “Generally Recognized as Safe”, and it is used as a food additive, in pharmaceutical formulations and cosmetics.^{13,14}

In 2007, we pioneered the preferential functionalization of the external surface of MSN, removal of the structure-directing agent, and drug loading of pores.¹⁵ The mesoporous silica, obtained from double-phase emulsions,¹⁶ externally derivatized with FOL, fluoresceine isothiocyanate and cisplatin-loaded, showed receptor-mediated uptake and cell killing in FR+ MM cells, without uptake in FR-negative (FR–) cells.¹⁷

Here, we describe the development and optimization process of an MSU-type mesoporous silica-based nanodevice, functionalized with folic acid and bearing the anticancer drug bortezomib linked through a pH-sensitive bond. Bortezomib is a synthetic compound approved by the US FDA for multiple myeloma (MM) patient treatment.¹⁸

The choice of using folic acid as a targeting function comes from the well-documented evidence that the folate receptor is highly expressed in tumor cells, including MM cells, compared with normal cells. Moreover, folic acid has been largely acknowledged as an effective targeting function to be exploited in drug-delivery nanosystems.¹⁹

The overall system engineered in order to be recognized and internalized by FR+ MM cells provides drug release when triggered in the acidic tumor microenvironment²⁰ and/or by the low pH²¹ of the endosomal vesicles during MSN cell internalization.

An accurate optimization process for the device, based on drug release at different pH and toxicity on healthy cells, also supported by a preliminary *in vitro* study,²² provided a prototype showing striking selectivity towards FR+ cancer cells without toxicity toward FR– healthy cells. Finally, a careful study of the suspensions revealed the best formulation to administer to myeloma-bearing mice. The obtained *in vivo* results showed improvement in the therapeutic efficacy, lower bortezomib toxicity when administered through the nanodevices, trend to drug accumulation in tumors, and lower drug deposits in normal tissues if compared with conventional bortezomib chemotherapy.

Results

The device: design, development, and characterization

The FOL-MSN-BTZ prototype was designed with the aim of improving the performance of conventional BTZ-based chemotherapies, increasing tumor selectivity, and reducing drug diffusion and deposit in healthy tissues.

It is a totally engineered device (Fig. 1a) able to release bortezomib as a response to a pH stimulus received only in the acidic microenvironment of the tumor (Fig. 1b). Fig. 1a shows the representation of FOL-MSN-BTZ with evidence of functionalization structural details. The targeting ligand, folic acid is covalently bonded, *via* an amide bond, to an aminopropyl group preferentially linked to the external surface of the nanoparticles while bortezomib forms, with a diol linker mainly anchored to the internal pore silica surfaces, a pH-sensitive cyclic boronate ester (Fig. 1). The as-synthesized materials were functionalized before solvent extraction of the polyethylene glycol (PEG)-based surfactant thus protecting the internal silica surface of the pores and, at the same time, preferentially addressing the aminosilane-modifying agent on the external surface of the mesoporous particles. According to this specific synthetic protocol, as previously reported, a considerable pore volume was recovered after the surfactant extraction from the PEG-templated folic acid-functionalized hybrid mesoporous silica. Folic acid was covalently linked on the external surface in a way that it neither blocked the pore entrances nor substantially filled the pores, allowing a relevant drug loading. Aminopropyl-functionalized particles (AP-MSN) were prepared by covalent grafting of (3-aminopropyl)triethoxysilane (APTES) on the MSN surface. Folic acid-functionalized nanoparticles (FOL-MSN) were then obtained by amide bond formation between the amino group of AP-MSN and folic acid carboxylic function (Fig. 2a). After the surfactant removal, the subsequent synthesis steps concerned BTZ-prodrug grafting through a pH-sensitive bond on the silica pore wall surface (Fig. 2b). The nanostructure FOL-MSN-BTZ was developed and successively optimized until negligible drug release at neutral pH was obtained. The optimized composition showed a lack of toxicity of FOL-MSN-BTZ *in vitro* towards healthy cells at physiological pH.

The drug release as a function of time from three different FOL-MSN-BTZ mesoporous silica compositions was studied. The analysis was performed using HPLC at different pH values to test the pH-sensitive behavior of the device. The composition indicated as Low Folic (LF) showed significant toxicity towards healthy cells *in vitro* (Fig. 2c) corresponding to a bortezomib release, as evidenced in Fig. 2d. Other two different samples, Medium Folic (MF) and High Folic (HF) were developed for the purpose of reaching the ideal nanostructure composition that is characterized, as mentioned, by lack of toxicity on healthy cells and negligible bortezomib release at neutral pH. Fig. 2e shows that very small amounts of bortezomib were still released at pH 7 from the MF composition. The best performance was reached with the HF composition, as shown in Fig. 2c and f. The increase in the folic acid content on the external surface of





Fig. 1 Graphical representation of FOL-MSN-BTZ structure and mechanism of internalization. (a) FOL-MSN-BTZ with evidence of functionalization structural details; (b) mechanism of FOL-MSN-BTZ uptake in cancer cells: (1) interaction of the device through folic acid with folate receptors (FR) overexpressed in cancer cells; (2) internalization of FOL-MSN-BTZ only in cancer cells where bortezomib is released in response to tumor acidic microenvironment; (3) MM cell death; (4) healthy cells unaffected by FOL-MSN-BTZ administration.

the mesoporous silica particle produces a continuous folic acid coverage that prevents the covalent grafting of the diol linker and consequently of the BTZ prodrug on the external surface. Our hypothesis is that the BTZ prodrug grafted on the external surface would be less protected and more easily hydrolysable also due to the catalytic role of silica's external surface that could lead to faster cleavage of the bond between BTZ and silica nanoparticles by water molecules even at neutral pH.

This hypothesis was confirmed using energy dispersive X-ray analysis (EDAX) carried out on the surface of LF, MF, and HF samples (Fig. 2g–i). The B/Si elemental ratios are 0.027 for LF (Fig. 2g), 0.0047 for MF (Fig. 2h), and 0.0025 for the HF prototypes (Fig. 2i). Corresponding polychromatic elemental maps of B and Si are reported in the energy-dispersive X-ray analysis provided in the ESI,[†] Results and discussion. The decrease of bortezomib prodrug content on the external surface of the particles is related to the increase of the folic acid content, which results, at the same time, in a reduction of

the drug release at neutral pH and toxicity to normal cells. Hereafter, we will refer to FOL-MSN-BTZ to indicate the optimized prototype (composition HF-MSN-BTZ) that exhibits an optimal drug release profile.

Transmission electron microscopy (TEM) micrographs (Fig. 3a and b) show that both the samples, MSN (Fig. 3a) and FOL-MSN-BTZ (Fig. 3b), exhibit a porous texture in adherence with materials of the MSU family, with dimensions of primary particles in the range between 80–120 nm.

Scanning electron microscopy (SEM) micrographs (Fig. 3c and d) show that this synthesis and successive modification procedures yielded nanoscaled particles without a regular morphology appearing also as aggregates of up to 300 nm.

All MSN samples highlighted a broad single reflection arising from the lack of long-range crystallographic order (Fig. 3e). This behavior is due to disorder in the assembly of the surfactant-templated channels in adherence to the patterns observed for the MSU materials.²³



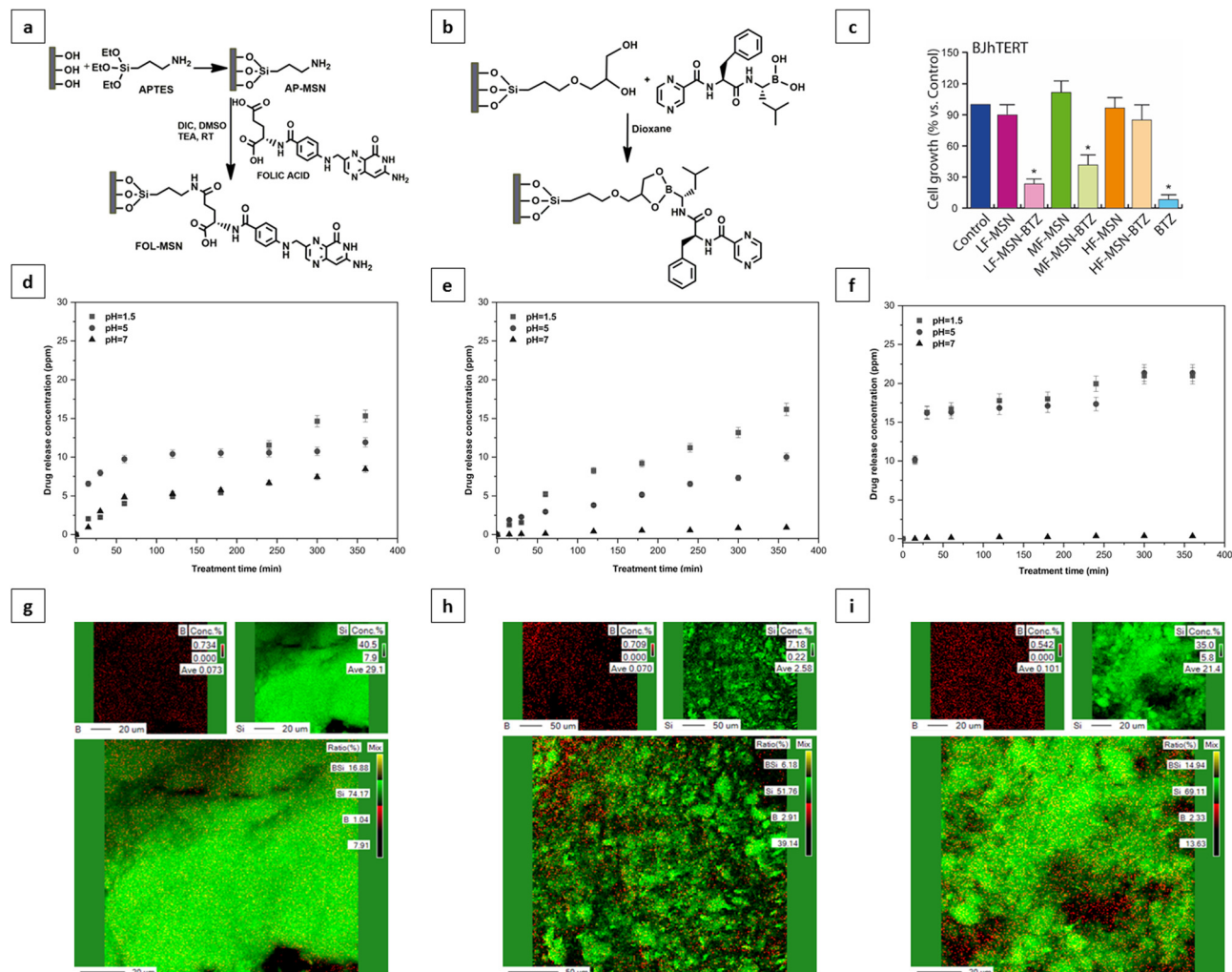


Fig. 2 Development details of FOL-MSN-BTZ nanodevice and nanostructure optimization (a) schematic representation of folic acid conjugation to the external surface of surfactant – bearing MSNs; (b) anchoring of BTZ, after surfactant removal, on the FOL-MSN inner pore walls, functionalized with a 1,2-diol linker, through the formation of a pH-sensitive cyclic boronate ester; (c) toxicity evaluation of LF, MF, and HF samples on normal BJhTERT cells: free BTZ was used as a positive control. Viability was determined after 3 days. Statistical analysis was performed using One-way ANOVA and data were reported as the mean \pm SD of 3 independent experiments, each performed in triplicates ($*p < 0,05$). Bortezomib release as a function of time, at different pH values from (d) LF-, (e) MF-, and (f) HF-composition of FOL-MSN-BTZ; EDAX elemental mapping of B, Si, and B/Si ratio in (g) LF, (h) MF and (i) HF FOL-MSN-BTZ samples.

Fig. 3f and g show nitrogen adsorption-desorption isotherms at 77 K and pore size distributions of FOL-MSN, FOL-MSN ext (surfactant-free FOL-MSN), and FOL-MSN-BTZ. The similar patterns observed for FOL-MSN and FOL-MSN-BTZ are due to the pore filling by surfactant micelles and BTZ prodrug, respectively. The FOL-MSN ext sample exhibited a higher pore volume due to surfactant extraction. Pore volume values shown (Fig. 3h) reflect pore size distributions (Fig. 3g). DLS characterization data (Fig. 3i) show a hydrodynamic diameter of around 344 and 373 nm for MSN and FOL-MSN-BTZ, respectively, assigned to the aggregates observed in SEM and TEM micrographs (Fig. 3b–d). Zeta potential values of MSN and FOL-MSN-BTZ are -30.2 ± 6.39 mV and 18.1 ± 3.41 mV respectively (Fig. 3i). The changes observed are related to the successful functionalization of the nanoparticles' surface²⁴ (refer to zeta

potential analysis in the ESI[†] Results and discussion for details).

Solid-state ²⁹Si and ¹³C NMR analysis of FOL-MSN-BTZ (Fig. S1, ESI[†]) confirmed the conjugation of the organic ligands and BTZ to the silica nanostructure. ¹³C NMR spectrum shows characteristic resonances that can be associated with the carbon atoms of the alkyl chains linked to the silicon²⁵ and the carbon atoms of FOL and BTZ.

FOL-MSN-BTZ selectively kills FR+ cancer cells

The obtained three different synthetic compositions of FOL-MSN-BTZ (LF-MSN-BTZ, MF-MSN-BTZ, HF-MSN-BTZ) were also tested on the human FR α -/FR β + MM RPMI cell lines (Fig. 4a). Interestingly, the specificity towards FR+ cells increased proportionally to the increase in the content of FOL on MSNs.





Fig. 3 Physico-chemical characterization of MSN samples. TEM micrographs of (a) starting MSN and (b) the complete nanocarrier FOL-MSN-BTZ. SEM micrographs of (c) MSN and (d) FOL-MSN-BTZ. (e) XRD powder diffraction patterns. (f) Nitrogen adsorption-desorption isotherms. (g) Pore-volume distributions. (h) BET surface area and pore volume at $P/P_0 = 0.96$ of the MSN derivatives obtained in the FOL-MSN-BTZ development process. (i) Hydrodynamic diameter, polydispersity index (Pdl), and zeta potentials of the starting MSN and the final FOL-MSN-BTZ; analysis were performed in triplicate, and the results are expressed as mean \pm standard deviation.

Therefore, while LF-MSN-BTZ showed similar toxicities on both FR+ RPMI (Fig. 4a) and normal FR- BJhTERT cells (Fig. 2c), MF-MSN-BTZ and HF-MSN-BTZ gradually showed increased selectivity towards FR+ RPMI cells. In particular, HF-MSN-BTZ did not show any significant toxicity on FR- BJhTERT cells. As expected, from our previous results,^{17,21} the vehicle alone (LF-MSN, MF-MSN, and HF-MSN) was not toxic to both normal or cancer cells (Fig. 2c). The effect of HF-MSN-BTZ and the corresponding precursor HF-MSN (*i.e.* FOL-MSN-BTZ and FOL-MSN, respectively) on cell proliferation was evaluated on FR- cell lines, and FR+ RPMI MM cells being BTZ the treatment of choice for this type of cancer. Strikingly, FOL-MSN-BTZ was able to selectively induce death or inhibit proliferation of FR+ tumor cells, but not in FR- normal cells, while free BTZ was not sign selective and resulted toxic for all cell lines tested, independently on their FR expression. These results fit very well with our TEM observations on RPMI and BJhTERT cells treated

with FOL-MSN-BTZ, which showed how MSNs are able to enter FR+ RPMI only and not FR- BJhTERT cells, where they remained confined in the intercellular spaces (Fig. 4b). Immunogold labelling experiments on RPMI confirmed that FOL-MSN-BTZ uptake occurs through the FR-mediated endocytosis (Fig. 4c).

***In vivo* administration of the smart chemotherapy: biocompatibility and antitumor efficacy**

Due to the sedimentation process of the particles that reduce their concentration in the suspensions and consequently the concentration of the drug, we have studied in detail the FOL-MSN and FOL-MSN-BTZ suspensions with the aim of developing the proper *in vivo* administration protocol. The protocol should take into account that the real drug amount that the mice were receiving was lower than the nominal concentration of the suspensions (see below: Materials and methods, *in vivo*



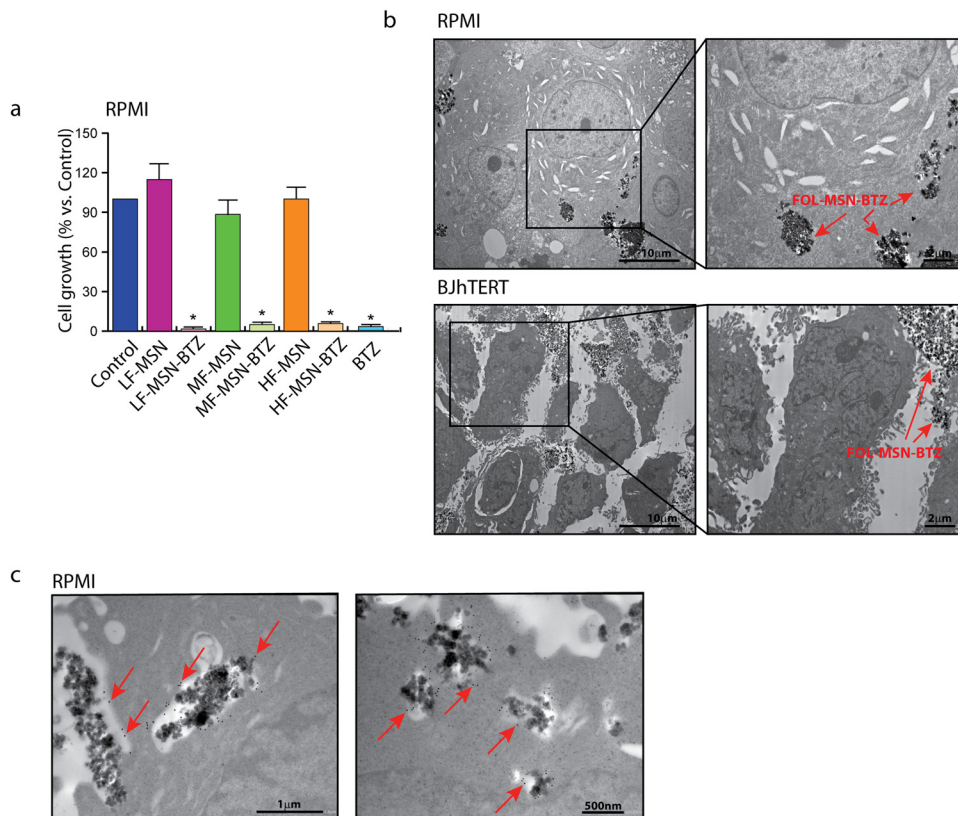


Fig. 4 MSN cellular uptake depends on FR expression. (a) FR+ RPMI MM cells were treated or not with LF, MF, and HF samples. Free BTZ was used as a positive control. Viability was determined after 3 days. Statistical analysis was performed using One-way ANOVA and the data are reported as the mean \pm SD of 3 independent experiments, each performed in triplicates ($*p < 0.05$). (b) TEM investigation on cancerous RPMI and normal BJhTERT cells after 1 h treatment with FOL-MSN-BTZ. Nanoparticles (arrows) enter FR+ RPMI only and not enter FR- BJhTERT cells. (c) Colloidal-gold immunocytochemistry for FR- β (black dots indicated by arrows) in RPMI cells exposed to FOL-MSN-BTZ for 1 h. The FR recognition at the cell membrane (left panel) and the sequestration in FR-immunopositive intracellular vesicles (right panel) are shown.

studies, and smart chemotherapy administration). Thus, the stability of the suspensions obtained according to the developed protocol was monitored in the time interval immediately preceding the injection. The stability analysis results show that, although a linear decrease in stability was observed, the correct administration of the selected doses was ensured in the first 10 minutes. The biodistribution and fate of MSNs were correlated to their physicochemical properties and to the medium in which they were suspended.²⁶ The evolution of nanoparticles over time and fate *in vivo* remains undefined.²⁷ (ESI,† Results and discussion).

A repeated dose range-finding toxicity study (No Observed Adverse Event Level, NOAEL) for FOL-MSN and FOL-MSN-BTZ was performed on healthy mice (Fig. 5a) to assess the most efficacious concentration of the nanodevice to be employed in the subsequent *in vivo* efficacy study. FOL-MSN showed outstanding tolerability at all tested doses, throughout the treatment period (Fig. 5a). In fact, it did not cause any significant reduction in body weight, or signs of general toxicity, in treated animals compared to controls. Moreover, mice well tolerated FOL-MSN-BTZ up to the dose of 2 mg kg^{-1} (*i.e.* MSNs bearing an amount of BTZ equal to 2 mg kg^{-1} (BTZ EQ), see Tables 1 and 2), but did not tolerate the highest dose (3 mg kg^{-1} BTZ EQ),

thus, for ethical reasons, these animals were sacrificed after the first administration. However, since the highest dose of the vehicle FOL-MSN (3 mg kg^{-1} BTZ EQ) was tolerated, we can conclude that the toxicity of FOL-MSN-BTZ 3 mg kg^{-1} (BTZ EQ), was due to the activity of BTZ itself and not to the nature of the vehicle (Fig. 5a), confirming, also *in vivo*, the safety and biocompatibility of the nanocarrier.

This result leads to the first important conclusion: animals tolerated a double dose of BTZ (2 mg kg^{-1} BTZ EQ) when the drug was delivered through the MSN platform if compared to the free drug formulation, for which the assessed maximum-tolerated dose was 1 mg kg^{-1} BTZ.¹⁸ Therefore, we expect that our pH-triggerable DDS, by protecting a double dose of the drug from premature release, will improve the therapeutic efficacy of BTZ towards the tumor.

Once identified FOL-MSN-BTZ 2 mg kg^{-1} (BTZ EQ) as the highest tolerated dose with no adverse observable events, we evaluated the efficacy of the nanodevice using an *in vivo* female SCID mice subcutaneous tumor (RPMI 8226 cells) model. Briefly, the mice were treated intravenously once a week for 5 weeks with FOL-MSN-BTZ 2 mg kg^{-1} (BTZ EQ), FOL-MSN 2 mg kg^{-1} (BTZ EQ), and BTZ 1 mg kg^{-1} used as the reference drug.²⁸ Our results showed that all the mice well-tolerated the MSN



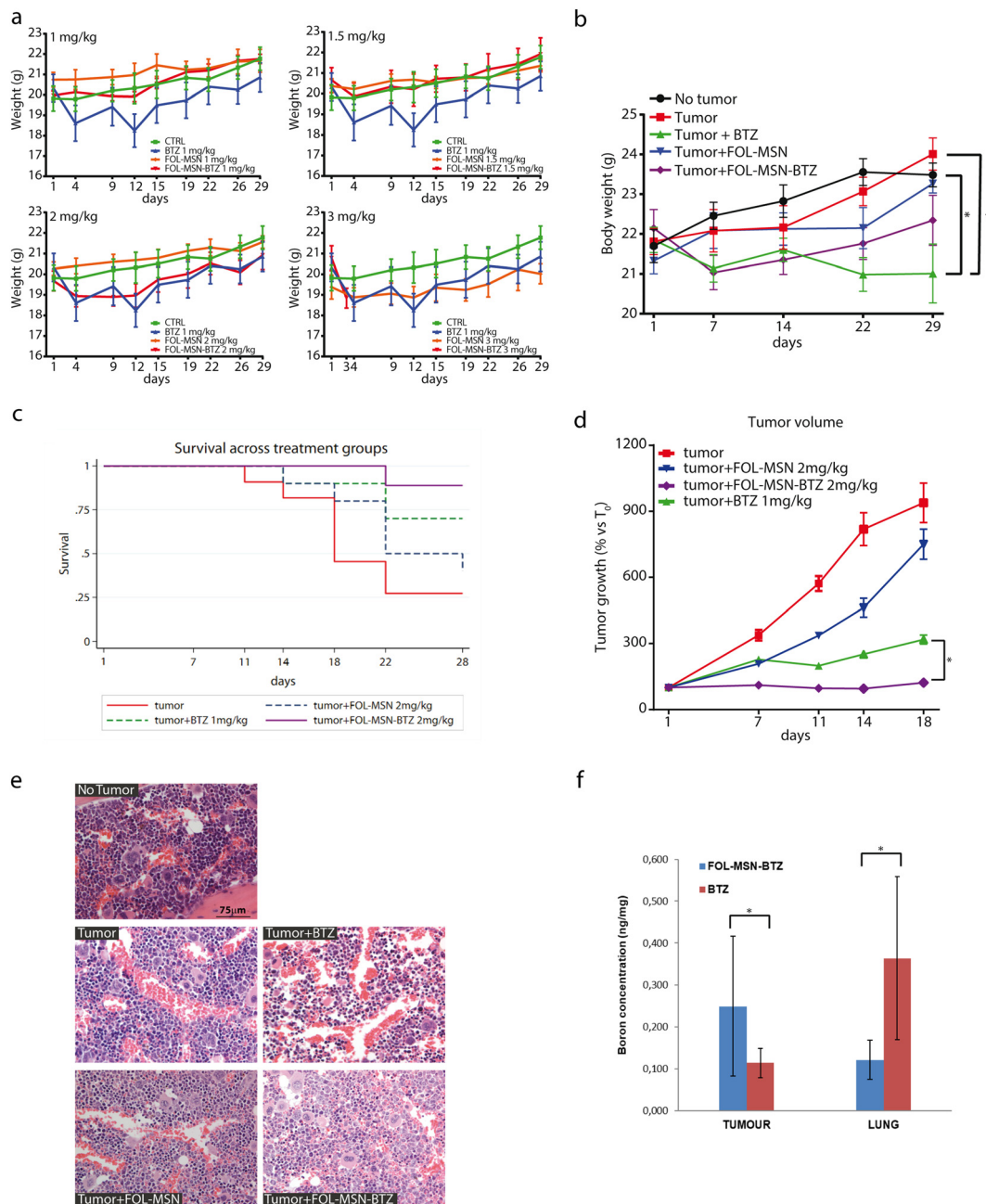


Fig. 5 Antineoplastic efficacy. (a) NOAEL for FOL-MSN and FOL-MSN-BTZ at indicated concentrations has been evaluated on healthy mice to assess the optimal dose to be employed in the efficacy study. (b) Body weight gains in mice throughout the treatment period. (c) Kaplan–Meier curves for survival analysis according to different treatment groups. (d) Percentage of increase (ratio between the tumor volume at each time point and the tumor volume at time 0) of tumor mass for each group. The results are expressed as mean \pm SD and were statistically analyzed using the analysis of variance (ANOVA) and the Tukey–Kramer post-test ($*p < 0.05$). (e) Effect of treatments on bone marrow. Representative images of sternum sections collected from the indicated treatment groups are reported. Captures were taken at 20 \times magnification scale bar: 75 μ m. (f) Comparison of boron amounts in tumor and lung tissues of mice treated with FOL-MSN-BTZ and free BTZ statistically analyzed using the non-parametric Mann–Whitney U test ($*p < 0.05$).

treatments since no significant body weight loss was observed throughout the experiment. Otherwise, mice treated with BTZ 1 mg kg⁻¹ showed a significant reduction ($p < 0.05$) in body weight compared with the untreated no-tumor group as well as with the untreated tumor-bearing group at the end of the treatment (Fig. 5b).

Survival analysis indicated a significant mortality rate in the untreated animals, as compared to treated animals ($p = 0.013$), especially considering FOL-MSN-BTZ (Fig. 5c) while the median survival time for the untreated group was 18 days. Indeed, during the experiment, it was necessary to sacrifice some untreated animals for ethical issues (Table S3, ESI[†]), thus the



Table 1 Evaluation of effective BTZ concentration in the suspensions prepared for the smart chemotherapy administration

Sample	Measured % (BTZ sample/BTZ tot)	Theoretical % (BTZ sample/BTZ tot)	BTZ concentration (mg mL ⁻¹)	Sample recovery (%)	BTZ dose in 0.2 mL (mg)
FOL-MSN-BTZ ₁	32.2	50	0.13	64.4	0.026
FOL-MSN-BTZ ₂	36.8	50	0.15	73.6	0.030
FOL-MSN-BTZ ₃	29.9	50	0.14	59.8	0.028
Avg.	22.9		0.14	65.9	0.028
St. dev.	3.5		0.01	5.8	0.002

Table 2 Corresponding FOL-MSN-BTZ and FOL-MSN concentrations for *in vivo* drug administrations

BTZ EQ concentration (mg kg ⁻¹)	FOL-MSN-BTZ concentration (mg kg ⁻¹)	FOL-MSN concentration (mg kg ⁻¹)
1.0	14.6	13.1
1.5	21.9	19.6
2.0	29.2	26.2
2.5	36.5	32.7
3.0	43.8	39.3

sample size of the untreated group progressively decreased. For this reason, and in order to have an adequate number of animals for each group, we performed the statistical analyses up to the 18th day (refer antitumor efficacy in the ESI,† Results and discussion for details). Mice treated with free BTZ showed only a slight increase in tumour volume during the whole experiment, confirming the anti-neoplastic effect of the drug (Fig. 5d). Notably, FOL-MSN-BTZ was able to completely stop the tumour growth as soon as after the first administration and throughout the treatment period. These data strongly show the higher efficacy of our delivery system compared to the free BTZ (Fig. 5d).

It is also worth mentioning that, although not statistically significant, the average tumor volumes in the FOL-MSN treated group were smaller than those in the untreated control animals at all time points. This intrinsic antitumor effect of FOL-targeted MSNs on tumor mass has already been observed by other authors²⁹ and could be referred to as FOL-MSN accumulation at the tumor site, supposedly due to FR recognition³⁰ and to the enhanced permeability and retention (EPR) effect.³¹ This result could also be due to the beneficial effect of both folic acid and mesoporous silica vehicles on fostering the immune system response.³²

Two days after the last administration, mice were sacrificed and blood samples were analyzed. No statistically significant differences were noticed among treated and not treated animals in all the hematochemical parameters (Fig. S6a, ESI†). The leukocyte formula showed a statistically significant increase ($p < 0.01$) in granulocyte counts in tumor-bearing mice treated with FOL-MSN-BTZ 2 mg kg⁻¹ (BTZ EQ) compared to mice without tumor or tumor untreated animals. Such an increase is clearly due to the drug, which, very likely, concentrates in the tumor site triggering sustained immunogenic cell death (ICD). In fact, bortezomib, by increasing ROS and ER stress, is one of the few chemotherapeutic drugs that have been recognized as an ICD inducer.^{33,34} ICD is associated with the chronic release

and/or exposure of damage-associated molecular patterns (DAMPs) by some dying apoptotic cells (e.g. tumor cells). DAMPs act as danger signals, eliciting immunostimulatory effects, including the recruitment and activation of macrophages, neutrophils, and other immune cells,³⁵ thus promoting immune-mediated elimination of tumor cells. This hypothesis would justify the increase in granulocyte count in FOL-MSN-BTZ treated mice (Fig. S6b, ESI†).

Tumor-bearing mice treated with BTZ and FOL-MSN-BTZ showed hepatic toxicity (GPT/ALT increase) compared to tumor not treated animals and mice without tumors (Fig. S6c, ESI†).

Nevertheless, the histological analysis of the liver tissue sections did not show any sign of injury in all the treatment groups, including FOL-MSN-BTZ (Fig. S7, ESI†). However, this effect is not surprising, considering the detoxification function of the liver. In fact, in large clinical trials of BTZ, elevations in serum aminotransferase levels were common, occurring in ~10% of patients, but the effect is transitory and normal values are restored after the treatment cycles.³⁶

Renal functionality was not affected by any treatment as confirmed by renal marker values (Fig. S6d, ESI†) and histological analysis (Fig. S7, ESI†). Mild hypoplasia was solely observed in the bone marrow of BTZ-treated mice (Fig. 5e), while no pathological alterations were noticed in the organs explanted from all the other experimental groups.

Moreover, boron and silicon, coming from BTZ and silica nanoparticles, respectively, have been dosed by ICP-MS in the tissues obtained from different organs 48 h after the last administration. Fig. 5f and Fig. S8 in the ESI,† present all the statistically significant data obtained.

The spleen, sternum, bladder, uterus, heart, and brain were collected and analyzed, for boron and silicon content. The obtained results have not been reported since no statistical analysis could be conducted due to the very low or even undetectable Si and B content found in these tissues.

As depicted in Fig. 5f, FOL-MSN-BTZ displayed a slightly higher accumulation in tumor tissue compared to free BTZ and this trend well fits with the higher *in vivo* antitumor efficacy of the developed platform, very likely due to its targeting capacity. Noteworthy, FOL-MSN-BTZ distribution in lungs was lower than the free BTZ, and this could represent a signal of the general lower diffusion and accumulation of the drug, if administered through FOL-MSN-BTZ nanodevice, in the different tissues of the organism, in comparison to the free drug but also to the excretion of FOL-MSN-BTZ that carries the drug away in the inactive form.



Higher silicon accumulation was detected in the liver tissue of mice treated with FOL-MSN-BTZ compared to the same tissue of mice treated with free BTZ, probably due to the role of the liver as the primary organ of the nanoparticle detoxification³⁷ (Fig. S8, ESI†). Conversely, no significant difference ($*p > 0.05$) in silicon accumulation was recorded in the kidney of untreated mice (CTR TUM), treated with FOL-MSN-BTZ, and FOL-MSN. Silicon detected in tissues of untreated mice (CTR TUM) and treated with free BTZ is related to the natural presence of this element in various organs as reported in the literature.³⁸

Conclusions

Here, we described a totally engineered approach to the development of an MSN-based nanodevice able to provide the smart administration of a chemotherapeutic agent. The system is engineered to be internalized by myeloma cells and to release BTZ only at a slightly acid pH, maintaining the drug in an inactive form at physiological pH and also in the case of direct excretion. Furthermore, it is designed to leave healthy cells unaffected. The fine balancing of the different functionalities of the nanodevice around the external and internal surface of the MSN particles was investigated with the aim of identifying an optimized nanostructure owning the most suitable features for target therapy applications.

The obtained nanodevices were engineered as injectable suspensions, which allowed the delivery of up to double the maximum administered dose of bortezomib in a MM animal model. This expectedly leads to a clear gain in therapeutic efficacy compared to the free drug. Noteworthy, the higher antitumor efficacy is not accompanied by higher toxicity, but rather a trend towards lower toxicity was observed. Indeed, compared to free bortezomib, FOL-MSN-BTZ-treated animals tended to live longer, did not significantly lose weight, and did not show marrow aplasia. Moreover, BTZ delivered through the nanodevice preferentially accumulates in tumors (very likely the reason for the higher efficacy of our system) and much less in other tissues.

The evidence gathered here shows the striking specificity of FOL-MSN-BTZ toward FR-expressing MM cells, a significantly higher *in vivo* antitumor efficacy, and a better safety profile compared to conventional bortezomib formulations. Our data suggest that FOL-MSN-BTZ represents a great opportunity for the future exploitation of MSNs-based strategies in the therapeutic management of multiple myeloma.

Materials and methods

Chemicals and reagents

Reagents were commercially available with analytical grade and used as purchased without further purification. Solvents were purified according to well-known laboratory methods and freshly distilled before use. Triton X-100, neutral polyoxyethylene (10) octylphenyl ether, tetraethylorthosilicate (TEOS),

(3-aminopropyl)-triethoxysilane (APTES), folic acid (FOL), diisopropylcarbodiimide (DIC), water (HPLC grade), acetone (HPLC grade) were purchased from MERCK/Sigma-Aldrich (Milan, Italy). Bortezomib was purchased from LC Laboratories, Woburn, MA. Ethanol, diethyl ether, 1,4-dioxane, dimethylformamide (DMF), tetrahydrofuran (THF), trifluoroacetic acid (TFA), and acetic acid were obtained from VWR. Dimethyl sulfoxide (DMSO) and cyclohexane were purchased from Merck and triethylamine from Carlo Erba. Ultrapure water was distilled using the MilliQ[®] water, Millipore.

Instruments and general experimental details

Thermogravimetric analysis (TGA) was carried out using a Netzsch STA 409 instrument between 293.15 K and 1123.15 K at a ramp of 10 K min⁻¹ in the air with a flow rate of 10 mL min⁻¹. The zeta potential values were determined using the Zeta-sizer ZS (Malvern Instruments Ltd, Malvern, U.K.) at 298.15 ± 0.1 K. The size and distribution of MSNs were determined, at 298.15 ± 0.1 K using Dynamic Light Scattering (DLS) analysis using a 90 Plus Particle Size Analyzer (Brookhaven Instruments Corporation, New York, USA).

NMR spectra were obtained at 300 K on a Bruker spectrometer Avance II 400 MHz.

²⁹Si {¹H} CP-MAS NMR spectra were recorded at 300 K on a Bruker spectrometer Avance II 400 MHz (9.4 T), operating at 79.4 MHz for ²⁹Si nuclide with a rotation rate of magic-angle of 6 KHz, 1000 scans, contact time 8 ms, a proton pulse of 5.1 ms and delay time of 5 s. Optimization of the Hartmann–Hahn condition was performed using a standard sample of Q8M8 (Si[CH₃]₃)₈Si₈O₂₀). ¹³C {¹H} CP-MAS NMR spectra were obtained at 300 K and 100.63 MHz for nuclide ¹³C with a rotation magic angle rate of 6 MHz, 4096 scans, a contact time of 2 ms, a proton pulse of 5.1 ms and a delay time of 3 s. Optimization of the Hartmann–Hahn condition was performed using a standard adamantane sample. All the samples were pressed using a zirconia rotator of 4 mm with Kel-F caps.

Determination of boron content was performed using atomic absorption spectroscopy on an Analytik.

Jena AG contraA 700 – High-Resolution Continuum Source Atomic Absorption Spectrometer. HPLC analyses for the release tests were performed on a Jasco HPLC analyzer using a flow rate of 1 mL min⁻¹. A 30/70% v/v of a solution of acetonitrile/water was used as the mobile phase. A UV-VIS wavelength of 270 nm was chosen to acquire the HPLC chromatograms.

Bortezomib release from FOL-MSN-BTZ was monitored, as a function of time, after keeping the suspension in physiological solutions at pH 7 typical of a haematic environment, pH 5 typical of intracellular organelles of cancer cells and pH 1.5, a strong acid pH, which is useful for the evaluation of the amount of bortezomib not hydrolysed at pH 5 that could be considered retained in the nanoparticles.

Synthesis of FOL-MSN-BTZ

MSN synthesis. The starting MSU-type MSNs, already employed in ref. 17, were synthesized at room temperature through a modification³⁹ of a previously-introduced interfacial



biphasic emulsion assembly mechanism at neutral pH of non-ionic poly(ethylene oxide)-based surfactants and silica.¹⁶

The surfactant Triton X-100 (21 g) was dissolved in ultrapure water (230 g) for about four hours at room temperature. In order to create two phases, along the vessel, it was slowly added to a solution of TEOS (22 g) in cyclohexane (9.8 g) (molar composition TEOS:cyclohexane:Triton X-100:H₂O was 1:1.08:0.32:120, respectively).

The synthesis was carried out at room temperature. The upper phase was removed and the resulting precipitate was collected by filtration and washed three times with ultrapure water. Finally, the sample was dried in the oven at 343.15 K for 24 h thus a white powder was obtained.

Synthesis of FOL-MSN. For this purpose, (3-amino-propyl)triethoxysilane (APTES) was used as an amino-silane linker at two different APTES:MSN ratios, AP-MSN(1) was at 2.03 g g⁻¹ and AP-MSN (2) was at 2.43 g g⁻¹. In a typical preparation, a solution containing APTES in ethanol (0.57 g mL⁻¹) was added to a suspension of (8 g) MSNs in (28.57 mL) of ethanol. The synthesis was left under stirring at room temperature for 48 h. The suspension was filtered and washed once with ethanol and twice with ultrapure water. The resulting solid sample (AP-MSN) was then placed in an oven at 343.15 K for 24 hours.

Three different FOL-MSN samples were synthesized using different FOL/AP-MSN ratios, LF-FOL-MSN, MF-FOL-MSN, and HF-FOL-MSN equal to 0.11, 0.12, and 0.14 g g⁻¹, respectively. Specifically, AP-MSN (1) was employed as starting material for LF-FOL-MSN, while AP-MSN (2) for MF-FOL-MSN and HF-FOL-MSN.

For the functionalization process, folic acid was used in combination with triethylamine (TEA) and *N,N'*-diisopropylcarbodiimide (DIC) in a molar ratio of 1:1.6:10.15 mmol, respectively.

Folic acid was completely dissolved in DMSO (0.04 g mL⁻¹). After that, TEA, DIC, and finally AP-MSN were added. The so-obtained suspension was stirred at room temperature for 40 hours. Finally, the mixture was filtered and washed with dimethylformamide (DMF), dioxane, diethyl ether, and ultrapure water (once for each solvent). The resultant yellow powder (5 g) was dried and stored in sealed containers protected from light. Subsequently, the surfactant within the pores was removed at room temperature using 1 g of material in 0.33 L of ultrapure water. The number of extractions required to reach a complete surfactant removal was established by monitoring (by TGA) the total mass loss of the sample subjected to subsequent extraction and filtration steps until a constant value was reached. Then, the resulting FOL-MSN was washed with 1,4-dioxane and dried at 318.15 K overnight.

Bortezomib loading. The inner pores of FOL-MSN were functionalized with 3-glycidoxypropyltrimethoxysilane. A suspension of FOL-MSN (1 g) in 1,4-dioxane (30 mL) 3-glycidoxypropyltrimethoxysilane (2 mL) was added. The reaction mixture was kept under stirring at room temperature for 18 h. Then, the mixture was washed with dioxane and THF and filtered through nylon filters, the resulting powder was dried at

318.15 K. The recovered product was subsequently treated with a 0.001 N HCl solution (pH 2–3). The mixture was stirred at room temperature for 10 h. After this time, the reaction mixture was washed with ultrapure water and THF, filtered, and dried at 318.15 K to afford FOL-MSN-DIOL.

For the FOL-MSN-BTZ preparation, bortezomib was loaded using a FOL-MSN-DIOL:BTZ molar ratio of 1:1.5 on the basis of the 1,2-diol linker content on FOL-MSN determined by TGA.

The reaction was carried out under an inert atmosphere. FOL-MSN-DIOL was suspended in dry 1,4-dioxane and then BTZ was added. The reaction mixture was gently stirred at room temperature for 24 h; then the nanoparticles were filtered and washed three times with dry dioxane and three times with dry dichloromethane. The recovered liquid phase was concentrated under reduced pressure and used for a second drug loading cycle. The second drug loading procedure was performed by adding 10% of the initially used amount of the drug to the solution resulting from the first drug loading cycle. The reaction was left for 24 h at room temperature under gentle stirring (30 rpm). The final product (FOL-MSN-BTZ) was filtered and washed as previously described. The sample was then stored in sealed containers at 253.15 K to preserve the integrity of the drug.

Determination of bortezomib content in FOL-MSN-BTZ. The drug loading in FOL-MSN-BTZ was determined by quantifying boron, exclusively present in the BTZ molecule, using flame atomic absorption (AAF). The BTZ content in FOL-MSN-BTZ was 10.38%.

The sample was treated as described below:

(1) dried at low temperature in a water bath (temperature heating plate 323.15 K – bath temperature 311.15 K); (2) transferred into plastic containers; (3) treated with 0.6 mL HF (complete dissolution of the MSN powder was observed); (4) treated with 0.1 mL HNO₃; (5) the addition of 6.3 mL of ultrapure water (MilliQ-test 1) to reach the final 7 mL sample volume required for the spectrophotometric analysis. The obtained samples were analyzed by atomic absorption spectroscopy (contraA[®] 700, Analytikjena, Germany).

The same technique and procedure were employed for the determination of the drug amount in the suspensions (see below: Smart chemotherapy administration).

Cell culture and treatments

Human FR+ MM RPMI-8226 (RPMI) and FR– normal foreskin fibroblast BJhTERT were purchased from ATCC where they were authenticated. Cells were stored according to the supplier's instructions and used within 6 months after frozen aliquot resuscitations. RPMI cells were cultured in RPMI-1640 medium and BJhTERT in Dulbecco's Modified Eagle's Medium (DMEM), both containing 10% Fetal Bovine Serum (FBS), 100 IU mL⁻¹ penicillin/streptomycin (pen/strep) and 0.2 mM L-glutamine. All culture media and additives were obtained from Gibco™ (Life Technologies, Monza MB, Italy). Trypsin-EDTA solution 10×, formaldehyde, EtOH, tween80, and NP-40 were obtained from MERCK/Sigma-Aldrich (Milan, Italy). Mycoplasma negativity was tested monthly (PlasmoTest, Invivogen). For the cell



treatment, a ratio of 1 μg MSNs/ 10^5 cells was used based on titration experiments. Free BTZ was added as a positive control in amounts corresponding to the percentage of BTZ carried by FOL-MSN-BTZ.

Cell proliferation assays

MSN effect on cell proliferation was assessed by the trypan blue exclusion assay. Cells were seeded in triplicates for each condition, synchronized in serum-free media (SFM) for 24 h, and then treated for 1 h with MSNs. Cells were then switched to fresh growing medium plus 1% FBS and counted after 72 h. Cell viability was determined by Countess[®] II Automated Cell Counter (Invitrogen, Life Technology, IT), according to the supplier's instructions.

Transmission electron microscopy (TEM) and electron immunocytochemistry

For conventional TEM analysis and electron immunocytochemistry, cells were treated as described for growth experiments and harvested after 1 h of treatment to detect MSN uptake. All samples were routinely fixed, dehydrated, and resin-embedded using heat polymerization.

For indirect immunolabeling, grids were floated on drops of 1% bovine serum albumin (BSA) in PBS containing 0.02-M glycine at RT for 30 minutes to reduce nonspecific binding. Sections were then incubated with a rabbit polyclonal antibody against FR- β (1:10) (Invitrogen, cat#PA5-45768) at 277.15 K overnight. The grids were then transferred to 50 μL drops of secondary antibody conjugated to 10 nm gold particles for 1 h, at RT. Observations were performed under a Jeol JEM-1400 Plus electron microscope (Jeol Ltd, Tokyo, Japan) operating at 80 kV.

In vivo studies. The intravenous administration of the nanoparticles needed the preliminary development of a FOL-MSN-BTZ suspension preparation protocol for obtaining a well-known suspension volume/bortezomib amount ratio. To reach this level of knowledge, the suspension obtained from FOL-MSN-BTZ in 0.9% physiological solution was carefully examined to evaluate the real drug concentration during the administration phase. Three different suspensions (FOL-MSN-BTZ₁₋₃) of known concentrations were prepared by magnetic stirring for 13 minutes, and the supernatant, equivalent to the upper half volume of the suspension, was immediately collected and analyzed by atomic absorption spectroscopy, to evaluate the effective boron concentration that is equimolar to bortezomib in FOL-MSN-BTZ.

The results presented in Table 1 suggest that the BTZ content in the liquid phase is 65.9% ($\pm 5.8\%$) of the expected dose of FOL-MSN-BTZ resuspended with magnetic stirring for 13 minutes and immediately collected, without sedimentation.

Animals and ethical statements

10 weeks old female Balb/cOlaHsd mice and five weeks old female SCID mice (C.B-17/IcrHanHsd-Prkdcscid) were purchased from Envigo (Bresso, Italy).

All mice were housed under a 12:12 h light:dark cycle with food and water available *ad libitum*.

Animal studies were reviewed and approved by the Ethics Committee of the University of Milano-Bicocca and the Ministry of Health (approval numbers 919/2015-PR del 27/07/2015). The accreditation number of the laboratory used for animal studies is 08/2015-UT of 21/05/2015. The care and husbandry of animals were in conformity with the institutional guidelines in compliance with national (D.L.vo no. 26/2014) and international laws and policies (EEC Council Directive 86/609, OJ L 358, 1, Dec.12, 1987; Guide for the Care and Use of Laboratory Animals, U.S. National Research Council, 1996).

NOAEL (no observed adverse event level)

NOAEL was conducted on 10 groups of female Balb/c mice (6 mice/group), receiving MSN-FOL and FOL-MSN-BTZ, at increasing concentrations corresponding to doses 1, 1.5, 2, and 3 mg kg⁻¹ of free BTZ, as follows:

- (1) Not treated mice (controls);
- (2) Free BTZ (1 mg kg⁻¹);
- (3) FOL-MSN-BTZ (1 mg kg⁻¹),
- (4) MSN-FOL (1 mg kg⁻¹);
- (5) FOL-MSN-BTZ (1.5 mg kg⁻¹);
- (6) MSN-FOL (1.5 mg kg⁻¹),
- (7) FOL-MSN-BTZ (2 mg kg⁻¹),
- (8) MSN-FOL (2 mg kg⁻¹);
- (9) FOL-MSN-BTZ (3 mg kg⁻¹),
- (10) MSN-FOL (3 mg kg⁻¹).

BTZ was administered at a final concentration of 1 mg kg⁻¹, chosen on the basis of previous results.¹⁸

The drug was dissolved in 5% EtOH and dissolved in a warm bath (37 °C). 5% tween80 and saline were then added and the obtained solution was sonicated by immersion until complete clarification. FOL-MSN-BTZ and MSN-FOL were suspended in saline solution with a magnetic stirrer for 15 minutes and were tested at the concentrations of 1, 1.5, 2, and 3 mg kg⁻¹. 10 mL kg⁻¹ of all treatments were administered intravenously once a week for 5 weeks (1qwx5). Corresponding amounts of saline solution were fed to control mice.

In vivo antitumor efficacy

RPMI 8226 cancer cells were subcutaneously implanted in the left hip of 7 weeks old animals (10 \times 10⁶ cells per animal in 200 μL PBS). When the tumor reached 200–500 mg size (about 30–40 days after implant), mice were divided into 5 groups, randomized on tumor size:

- (1) No tumor ($n = 7$);
- (2) Untreated tumor ($n = 11$);
- (3) Tumor + BTZ 1 mg kg⁻¹ ($n = 10$);
- (4) Tumor + FOL-MSN 2 mg kg⁻¹ ($n = 10$);
- (5) Tumor + FOL-MSN-BTZ 2 mg kg⁻¹ ($n = 9$).

Based on NOAEL data (Fig. 5a), FOL-MSN and FOL-MSN-BTZ were used at 2 mg kg⁻¹, while BTZ was at 1 mg kg⁻¹.²⁶ BTZ was dissolved in 5% EtOH in a warm bath (310.15 K). 5% tween80 and saline were then added and the obtained solution was sonicated by immersion until complete clarification. FOL-MSN-BTZ and FOL-MSN were suspended in saline solution with a



magnetic stirrer for 15 minutes and were tested at the concentrations of 2 mg kg^{-1} .

All the treatments were administered intravenously at 10 mL kg^{-1} once a week for 5 weeks (1qwx5). Corresponding amounts of saline solutions were fed to control mice.

Animal general conditions were recorded daily until sacrifice. Changes in their appearance (decreased grooming, disheveled fur, piloerection, exaggerated kyphosis), behavior (decreased nesting), and activity (decreased exploring) were monitored daily. Mice's weight and tumor size were measured twice a week. The growth of subcutaneous tumors was measured using a Vernier caliper. The length (L) and width (W) of the tumors was measured and their volumes were calculated using the formula $(L \times W^2)/2$. Animals were sacrificed when tumor volume exceeded about 10% of their body weight.

Hematological, hematochemical, and histological analysis

48 h after the last administration, the mice were sacrificed and blood was analyzed for the hematochemical and hematological parameters.

48 h after the last administration, 3 mice/group were sacrificed and the main organs were collected for histological examinations. Some of the animals were sacrificed for ethical reasons at the end of the experiment, in case abnormal tumor growth occurred (Table S3, ESI†).

Once collected, the target organs were washed with 0.1 M PBS, pH 7.4, fixed by immersion in 10% buffered formalin O/N at room temperature, embedded in paraffin (Embedding Center Leica EG1160, Leica Biosystem, Wetzlar, Germany), cross-sectioned at $3 \mu\text{m}$ thickness by a rotary microtome, mounted on slides, stained using hematoxylin and eosin (HE) and observed under a light microscope (Nikon Eclipse 50i, Melville, NY, USA). Representative images were captured with a digital camera (Nikon Digital Sight DS-2Mv).

MSN biodistribution

Metal concentrations in tissues were measured by inductively coupled plasma-mass spectrometry (ICP-MS) analysis. The determinations were carried out utilizing an Elan DRC-e ICP-MS instrument (PerkinElmer SCIEX, Canada), and the sample delivery system consisted of a PerkinElmer autosampler model AS-93 Plus with a peristaltic pump and a cross-flow nebulizer with a Scott type spray chamber. The ICP torch was standard (Fassel-type torch) with a platinum injector. A solution containing Rh, Mg, Pb, Ba, and Ce ($10 \mu\text{g L}^{-1}$, Merck) was used to optimize the instrument in terms of sensitivity, resolution, and mass calibration.

An Anton Paar Multiwave 3000 with programmable power control (maximum power 1400 W) and rotor XF100 (operating pressure up to 120 bar maximum; operating temperature, 533.15 K maximum; construction material, PTFE-TFM for the liner) was used for the microwave digestion of samples. The digestion was achieved by adding 4 mL of HNO_3 and 2 mL H_2O_2 into vessels containing 100 mg of tissue with a power ramp from 0 to 600 W in 15 min , a 10 min hold step at 600 W , and a cooling step for 10 min . After digestion, the extracts were

quantitatively transferred to a graduated polypropylene test tube, diluted with ultrapure water to 50 mL , and then analyzed by ICP-MS.

Single element solutions of B and Si (100 mg L^{-1} , Merck) were used for the preparation of aqueous calibration standard solutions after appropriate dilution. For the quantitative analysis, external calibration curves were built on seven different concentrations in a calibration range of $0.2\text{--}500 \mu\text{g L}^{-1}$.

The comparison between the boron concentration values detected in tumour tissues of mice treated with free BTZ and FOL-MSN-BTZ was made by applying the non-parametric Mann-Whitney U test. The same statistical approach was applied to compare the boron concentrations found in lung tissue.

Statistical evaluation. We firstly assessed the survival of animals in different treatment groups using the Kaplan-Meier method, providing also the log-rank test for the comparison of estimated survivor failure functions. We set up death as the failure indicator (whether or not the animal was ethically sacrificed when the tumor volume reached a challenging value) and days from the baseline assessment to death or censoring as the time at risk according to the follow-up period of the study. We visually inspected tumor growth, considering log-transformed tumor volume and potentially-exponential growth. Descriptive statistics are provided (*e.g.*, median with interquartile range – iqr). The Kruskal-Wallis test was performed to test any differences in terms of animals' tumor volume at baseline. Taking into account repeated measures for the same animal, we performed a mixed-effects generalized linear model, with a random-intercept term at the animal level and specifying a Gamma distribution, to test the association between the treatment group and tumor volume (outcome). We also included the interaction between treatment groups and time to assess tumor growth differences over time according to different treatment groups. In addition, we assessed treatment group differences by estimating conditional marginal effects and performing pairwise comparisons of average marginal effects.

Body weight and hematochemical/haematological parameters were statistically analyzed using a 2-step approach involving a nonparametric One-way ANOVA test and the Kruskal-Wallis post-test (significance level set at $p < 0.05$). Data analysis was carried out using GraphPad 4.0 software (GraphPad Software, Inc., San Diego, California).

Author contributions

L. P. and A. L. formulated the conception and the aim of the work, L. P., A. L., and C. M. provided the acquisition of the financial support for the research and oversaw it, and wrote and critically revised the manuscript. M. D. S., A. G., I. E. D. N., and M. G. performed MSNs synthesis and physicochemical characterization, A. C. prepared intermediates and substrate for MSN synthesis, E. M. conducted DLS analysis, I. P. and M. D. carried out TEM and SEM analysis respectively. T. G. developed the HPLC methodology to study bortezomib release from



engineered nanoparticles at different pH. P. A. executed the AAF analysis and interpreted the data. A. T. performed ICP-MS analysis with the contribution of R. E. and conducted the statistical analysis of the acquired data. A. N. and M. F. conducted the *in vitro* studies, D. S. conducted the statistical analysis of the *in vitro* and *in vivo* data, and helped draft the manuscript. G. N. performed conceptualization and supervision of the *in vivo* studies, A. C. and S. S. conducted the *in vivo* studies, E. B. carried out the histopathological studies, C. C. conducted biostatistical analysis, G. C. supervised, analyzed, interpreted, and drafted the data of animal studies. L. P., A. L., and C. M. performed analysis and interpretation of the data, drafting the final manuscript with the contribution of M. D. S., A. G., E. M., D. S., G. C., and D. L. performed the final manuscript curation. All authors read and approved the manuscript before submission.

Data availability statement

The data supporting the findings of this study are available from the corresponding author upon reasonable request.

Conflicts of interest

NanoSiliCal Devices, a company founded by the authors L. P., A. L., and C. M., a spinoff of the University of Calabria, owns the Patent EP 3 288 955 B1 that claims, among other things, the prototype FOL-MSN-BTZ.

Acknowledgements

The research activities were funded by NanoSiliCal Devices's private financial support and related co-funded by Calabria National Operating Programme (NOP) 2007–2013 Project "TalentLab Spinoff" (FESR funds, Axis I), Calabria NOP 2014–2020 Projects "Research and Innovation" (ERDF-ESF funds, Axis I, Action 1.1.2), "R&D" (Axis I, Action 1.2.2), NOP "Research and Innovation" (Axis I, Action I.1) and by EU Horizon 2020-Research and Innovation Framework Program-SME-Instrument Phase I.

References

- 1 A. Rifai, N. Tran, P. Reineck, A. Elbourne, E. Mayes, A. Sarker, C. Dekiwadia, E. P. Ivanova, R. J. Crawford, T. Ohshima, B. C. Gibson, A. D. Greentree, E. Pirogova and K. Fox, Engineering the interface: nanodiamond coating on 3D-printed titanium promotes mammalian cell growth and inhibits *Staphylococcus aureus* colonization, *ACS Appl. Mater. Interfaces*, 2019, **11**, 24588–24597.
- 2 E. Rivero-Buceta, C. Vidaurre-Agut, C. D. Vera-Donoso, J. M. Benlloch, V. Moreno-Manzano and P. Botella, PSMA-targeted mesoporous silica nanoparticles for selective intracellular delivery of docetaxel in prostate cancer cells, *ACS Omega*, 2019, **4**, 1281–1291.
- 3 A. Nigro, M. Pellegrino, M. Greco, A. Comandè, D. Sisci, L. Pasqua, A. Leggio and C. Morelli, Dealing with skin and blood-brain barriers: The unconventional challenges of mesoporous silica nanoparticles, *Pharmaceutics*, 2018, **10**, 250.
- 4 C. Chircov, A. Spoială, C. Păun, L. Crăciun, D. Ficăi, A. Ficăi, E. Andronescu and Ş. C. Turcules, Mesoporous silica platforms with potential applications in release and adsorption of active agents, *Molecules*, 2020, **25**, 3814.
- 5 R. Mout, D. F. Moyano, S. Rana and V. M. Rotello, Surface functionalization of nanoparticles for nanomedicine, *Chem. Soc. Rev.*, 2012, **41**, 2539–2544.
- 6 R. Huang, Y. W. Shen, Y. Y. Guan, Y. X. Jiang, Y. Wu, K. Rahman, L. J. Zhang, H. J. Liu and X. Luan, Mesoporous silica nanoparticles: Facile surface functionalization and versatile biomedical applications in oncology, *Acta Biomater.*, 2020, **116**, 1–15.
- 7 R. Salve, P. Kumar, W. Ngamcherdtrakul, V. Gajbhiye and W. Yantasee, Stimuli-responsive mesoporous silica nanoparticles: A custom-tailored next generation approach in cargo delivery, *Mater. Sci. Eng.*, 2021, **124**, 112084.
- 8 M. Vallet-Regí, I. Colilla and M. Izquierdo-Barba, Manzano, Mesoporous silica nanoparticles for drug delivery: Current insights, *Molecules*, 2018, **23**, 1–19.
- 9 A. M. Mebert, C. J. Baglolle, M. F. Desimone and D. Maysinger, Nanoengineered silica: Properties, applications and toxicity, *Food Chem. Toxicol.*, 2017, **109**, 753–770.
- 10 W. X. Mai and H. Meng, Mesoporous silica nanoparticles: a multifunctional nano therapeutic system, *Integr. Biol.*, 2013, **5**, 19–28.
- 11 F. Tang, L. Li and D. Chen, Mesoporous silica nanoparticles: synthesis, biocompatibility and drug delivery, *Adv. Mater.*, 2012, **24**, 1504–1534.
- 12 W. H. Chen, G. F. Luo, W. X. Qiu, Q. Lei, L. H. Liu, S. B. Wang and X. Z. Zhang, Mesoporous silica-based versatile theranostic nanoplatform constructed by layer-by-layer assembly for excellent photodynamic/chemo therapy, *Biomaterials*, 2017, **117**, 54–65.
- 13 J. G. Croissant, Y. Fatieiev and N. M. Khashab, Degradability and Clearance of Silicon, Organosilica, Silsesquioxane, Silica Mixed Oxide, and Mesoporous Silica Nanoparticles, *Adv. Mater.*, 2018, **29**, 1604634.
- 14 <https://www.accessdata.fda.gov/scripts/cdrh/cfdocs/cfcfr/cfrsearch.cfm>.
- 15 L. Pasqua, F. Testa, R. Aiello, S. Cundari and J. B. Nagy, Preparation of bifunctional hybrid mesoporous silica potentially useful for drug targeting, *Microporous Mesoporous Mater.*, 2007, **103**, 166–173.
- 16 L. Pasqua, F. Testa and R. Aiello, Interfacial polycondensation of mesoporous silica particles at the nanometer scale, *Stud. Surf. Sci. Catal.*, 2005, **158A**, 557–564.
- 17 C. Morelli, P. Maris, D. Sisci, E. Perrotta, E. Brunelli, I. Perrotta, M. L. Panno, A. Tagarelli, C. Versace, M. F. Casula, F. Testa, S. Andò, J. B. Nagy and L. Pasqua, PEG-templated mesoporous silica nanoparticles exclusively target cancer cells, *Nanoscale*, 2011, **3**, 3198–3200.



- 18 C. Meregalli, V. A. Carozzi, B. Sala, A. Chiorazzi, A. Canta, N. Oggioni, V. Rodriguez-Menendez, E. Ballarini, C. Ceresa, G. Nicolini, L. Crippa, M. Orciani, G. Cavaletti and P. Marmiroli, Age-related changes in the function and structure of the peripheral sensory pathway in mice, *J. Biol. Regul. Homeostatic Agents*, 2015, **29**, 115.
- 19 L. Pasqua, A. Leggio, D. Sisci, S. Andò and C. Morelli, Mesoporous silica nanoparticles in cancer therapy: Relevance of the targeting function, *Minireviews Med. Chem.*, 2016, **16**, 743–753.
- 20 J. S. Burns and G. Manda, Metabolic pathways of the Warburg effect in health and disease: perspectives of choice, chain or chance, *Int. J. Mol. Sci.*, 2017, **18**, 2755.
- 21 C. Wang, T. Zhao, Y. Li, G. Huang, M. A. White and J. Gao, Investigation of endosome and lysosome biology by ultra pH-sensitive nanoprobe, *Adv. Drug Delivery Rev.*, 2017, **113**, 87–96.
- 22 A. Nigro, L. Frattaruolo, M. Fava, I. De Napoli, M. Greco, A. Comandè, M. De Santo, M. Pellegrino, E. Ricci, F. Giordano, I. Perrotta, A. Leggio, L. Pasqua, D. Sisci, A. R. Cappello and C. Morelli, Bortezomib-loaded mesoporous silica nanoparticles selectively alter metabolism and induce death in multiple myeloma cells, *Cancers*, 2020, **12**, 2709–2728.
- 23 S. A. Bagshaw, E. Prouzet and T. J. Pinnavaia, Templating of mesoporous molecular sieves by nonionic polyethylene oxide surfactants, *Science*, 1995, **269**, 1242–1244.
- 24 M. Chen, J. Hu, L. Wang, Y. Li, C. Zhu, C. Chen, M. Shi, Z. Ju, X. Cao and Z. Zhang, Targeted and redox-responsive drug delivery systems based on carbonic anhydrase IX-decorated mesoporous silica nanoparticles for cancer therapy, *Sci. Rep.*, 2020, **10**, 1–12.
- 25 A. Marchetti, J. Yin, Y. Su and X. Kong, Solid-state NMR in the field of drug delivery: State of the art and new perspectives, *Magn. Reson. Lett.*, 2021, **1**, 28–70.
- 26 G. Croissant, Y. Fatieiev, A. Almalik and N. M. Khashab, Mesoporous silica and organosilica nanoparticles: physical chemistry, biosafety, delivery strategies, and biomedical applications, *Adv. Healthcare Mater.*, 2018, **7**, 1700831.
- 27 N. Feliu, D. Docter, M. Heine, P. Del Pino, S. Ashraf, J. Kolosnjaj-Tabi, P. Macchiarini, P. Nielsen, D. Alloyeau, F. Gazeau, R. H. Stauber and W. J. Parak, *In vivo* degeneration and the fate of inorganic nanoparticles, *Chem. Soc. Rev.*, 2016, **45**, 2440–2457.
- 28 C. Meregalli, V. A. Carozzi, B. Sala, A. Chiorazzi, A. Canta, N. Oggioni, V. Rodriguez-Menendez, E. Ballarini, C. Ceresa, G. Nicolini, L. Crippa, M. Orciani, G. Cavaletti and P. Marmiroli, Bortezomib-induced peripheral neurotoxicity in human multiple myeloma-bearing mice, *J. Biol. Regul. Homeostatic Agents*, 2015, **29**, 115–124.
- 29 W. Cheng, J. Nie, L. Xu, C. Liang, Y. Peng, G. Liu, T. Wang, L. Mei, L. Huang and X. Zeng, pH-sensitive delivery vehicle based on folic acid-conjugated polydopamine-modified mesoporous silica nanoparticles for targeted cancer therapy, *ACS Appl. Mater. Interfaces*, 2017, **9**, 18462–18473.
- 30 B. Frigerio, C. Bizzoni, G. Jansen, C. P. Leamon, G. J. Peters, P. S. Low, L. H. Matherly and M. Figini, Folate receptors and transporters: biological role and diagnostic/therapeutic targets in cancer and other diseases, *J. Exp. Clin. Cancer Res.*, 2019, **38**, 125.
- 31 H. Maeda, J. Wu, T. Sawa, Y. Matsumura and K. Hori, Tumor vascular permeability and the EPR effect in macromolecular therapeutics: a review, *J. Controlled Release*, 2000, **65**, 271–274.
- 32 K. T. Mody, A. Popat, D. Mahony, A. S. Cavallaro, C. Yu and N. Mitter, Mesoporous silica nanoparticles as antigen carriers and adjuvants for vaccine delivery, *Nanoscale*, 2013, **5**, 5167–5179.
- 33 R. Spisek, A. Charalambous, A. Mazumder, D. H. Vesole, S. Jagannath and M. V. Dhodapkar, Bortezomib enhances dendritic cell (DC)-mediated induction of immunity to human myeloma via exposure of cell surface heat shock protein 90 on dying tumor cells: therapeutic implications, *Am. J. Hematol.*, 2007, **109**, 4839–4845.
- 34 A. Serrano-del Valle, A. Anel, J. Naval and I. Marzo, Immunogenic cell death and immunotherapy of multiple myeloma, *Front. Cell Dev. Biol.*, 2019, **7**, 50.
- 35 S. Nagata and M. Tanaka, Programmed cell death and the immune system, *Nat. Rev. Immunol.*, 2017, **17**, 333–340.
- 36 LiverTox: Clinical and Research Information on Drug-Induced Liver Injury. https://www.ncbi.nlm.nih.gov/books/NBK548027/?report=reader#_NBK548027_pubdet_.
- 37 Y. N. Zhang, W. Poon, A. J. Tavares, I. D. McGilvray and W. C. Chan, Nanoparticle–liver interactions: cellular uptake and hepatobiliary elimination, *J. Controlled Release*, 2016, **240**, 332.
- 38 N. P. Zaksas, S. E. Soboleva and G. A. Nevinsky, Twenty Element Concentrations in Human Organs Determined by Two-Jet Plasma Atomic Emission Spectrometry, *Sci. World J.*, 2019, **2019**, 9782635.
- 39 N. Garofalo, A. Comandè, I. Perrotta, M. Davoli, G. Niceforo and L. Pasqua, Synthesis and Characterization of Large Pore MSU-Type Mesoporous Silica, *Adv. Sci. Lett.*, 2017, **23**, 6026–6028.

